# Flow : a study of electron transport through networks of interconnected nanoparticles

Blok, S.

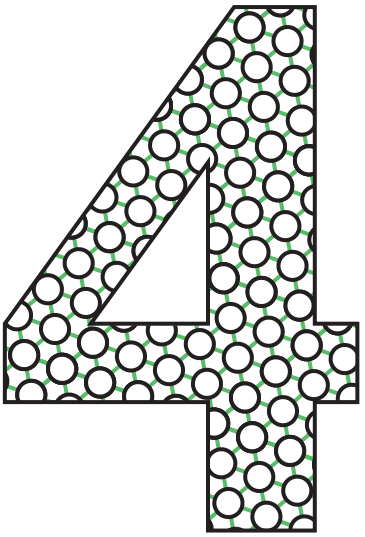

# Experimental set-up and sample fabrication

The goal of this research is to study electron transport through nanoparticle networks at low temperatures. As explained in the past few chapters, current through a Coulomb blockaded network is expected to be dominated by (multiple) cotunneling. This type of transport depends strongly on the external conditions, mainly temperature and applied bias. Studying it involves measuring the rate of transport, and therefore electrical current, as a function of applied bias and temperature. This electrical current is small, down to fA and lower, as cotunneling is a higher order process.

In order to study cotunneling in nanoparticle networks, they need to be Coulomb blockaded, and hence cooled down to low temperatures. For a nanoparticle size of 10 nm, this temperature is below 100 K. Moreover, this temperature needs to be stable within a few percent, as the cotunneling current depends strongly on temperature.

This combination of low currents and low but stable temperatures requires specialized equipment. With this in mind, a new cryostat was installed as part of this research. In addition to the cryostat, a new low-current measurement set-up was built partly in-house, integrating with the electromagnetic shielding that the cryostat provides. This chapter describes this set-up and discusses sample fabrication.

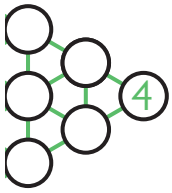


## 4.1 Cryostat

The cryostat used in this research is an Oxford Instruments Teslatron closed loop cryostat. It was installed as part of the research described in this thesis. The Teslatron enables conductance measurements at variable temperatures from 300 K down to 1.5 K. Furthermore, in contrast to a bath cryostat, its closed loop system requires no refilling of liquid helium and therefore enables continuous operation for months on end. A picture of the cryostat can be seen in Fig. 4.1. The outer casing is pumped to below $10^{-4}$ mbar to provide thermal insulation from the outside environment. Inside the cryostat are two sets of radiation shields to further separate the cryogenic temperature at the sample from the room temperature in the lab. The outer radiation shield is cooled down to between 40 K and 70 K, while the inside shield is cooled down even further to 4 K. The sample is positioned at the bottom of the cryostat using an insert. The insert provides electrical connections between the sample and the laboratory equipment, while additionally providing a thermocouple and heater element to control the sample temperature with 10 mK accuracy. The heart of the cryostat is a two stage pulse tube, the workings of which are explained in the appendix. It provides the cooling power necessary to investigate (amongst other things) cotunneling in nanoparticle networks. The sample itself is placed in the center of a superconducting magnet, enabling study in magnetic fields of up to 9 Tesla.




**Fig. 4.1:** Picture of the cryostat as installed. The rotary valve feeding the pulse tube can be seen on the top left, connected to two (one supply, one return) high pressure helium lines. The various lines in the top right are from right: insert vacuum line, helium circulation return (big line), helium circulation supply (small line).

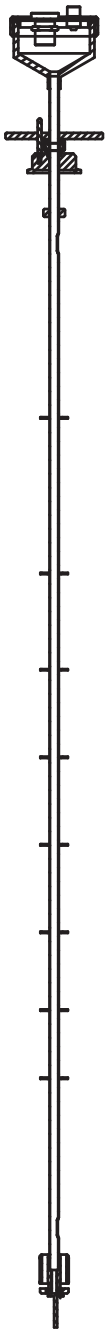

Fig. 4.2: Schematic of the insert as delivered by Oxford Instruments. After delivery, the wiring was replaced to reduce the noise floor. An alternative sample holder was fitted to enable illumination of the sample. Since the temperature sensor was originally fitted in the copper mass at the bottom, it was replaced by a sensor closer to the sample.

### 4.1.1 Remote operation and automation

The entire cryostat is controlled using a Mercury iTC (intelligent Temperature Controller), which has built-in algorithms to control the pressure at the needle valve, the temperature of the insert chamber, but also the temperature of the insert itself. Furthermore, the remote control capabilities allow full automation of the measurement procedure.

Automation software was written together with Isabelle Janssen[1]. The software was written in Python and can control the pressure and temperature and run a measurement script. As input, the software takes a configuration file, which contains a list of temperatures and measurement parameters. It then programmatically sets the setpoint temperature, waits for thermal stabilization and runs the measurement. Using a six-channel RF-switch*, up to six samples can be measured automatically at each temperature.

In order to increase the temperature settling speed at temperatures above 50 K, the needle valve is fully opened to allow optimal heat dissipation. Between 20 K and 50 K, the needle valve is closed halfway to decrease the heat load on the 4 K stage. Below 20 K, the needle valve is set to use pressure feedback to attain a pressure of 7 mbar, a value which was found to result in lowest sample temperature. A full cooldown to 1.6 K and warmup to room temperature cycle can take under 24 hours.

After temperature stability was reached, the chosen sample was connected automatically, and a LabVIEW script is called to perform the measurement. After the measurement, the program selects the next sample to measure, or set the next setpoint temperature after all samples are measured.

### 4.1.2 Insert

The cryostat cools down a small space at the bottom of the system. To measure a sample at these low temperatures, it needs to be thermally connected to the cold stage, while still being connected electrically to the measurement equipment. This is done by an insert; a long rod with connectors at the top, which electrically connect to the sample at the bottom, seen in Fig. 4.2.

To eliminate external interference in the current measurement, the insert was wired using low capacitance coaxial cables (85 pF $m^{-1}$, 170 μm core di-

* Radio Frequency switches are ideal for this application, as the leak resistance during open circuit is very large: >PΩ

ameter) by Bert Crama. At the bottom of the insert, the coaxial shields were soldered to the chassis of the sample holder, electrically connecting them. The wire cores were attached to individual connections on the sample holder, allowing the measurement of 12 devices simultaneously. The leak resistance was measured to be larger than a PΩ, which means that leakage currents have no significant effect on the measured signal, even at low temperatures and applied bias.

The cables added a significant amount of copper to the insert, and hence introduced a heat load on the sample. After wiring the insert, the base temperature increased by 100 mK to 1.6 K. Furthermore, the thermometer fitted by Oxford Instruments was positioned a few centimeters from the sample, introducing uncertainties in sample temperature. To correct this, a Lakeshore DT-670 silicon diode thermometer was fitted under the chip carrier, close to the sample. A picture of the insert can be seen in Fig. 4.3

**Fig. 4.3:** Picture of the low noise insert used in this research. The white coaxial cables go down to the sample through the copper mass containing the heater element. At the bottom, the shields are connected to the ground of the sample connector, and the wire cores are connected to individual pins. The optical fiber is the black wire sticking out. For the measurements, it was shortened and fixed above the sample, allowing illumination.

In order to allow illumination of the sample, a 600 μm core diameter glass fiber was fitted inside the insert. The bottom of the fiber was open ended and fixed 2 cm above the sample, ensuring complete illumination.

### 4.1.3 Chip carrier

In order to perform electrical measurements, the sample needs to be connected to the insert. This is done by a chip carrier. The carrier holds the sample and has electrical connecting pins that allow easy connection to the insert. Normally, the sample is connected to the carrier by wire bonds. However, making these bonds on the micrometer scale is tedious work, and can take hours per sample. Moreover, it requires a microscope and clear lighting to be feasible. As we shall see in chapter 6, some samples are sensitive to light, requiring wire bonds to be made in a darkened environment, vastly increasing the difficulty of this process. To ease the fabrication of electrical contacts to the on-chip devices to the carrier, we designed a two-piece carrier. The top piece (Fig. 4.4, right picture) holds eight spring contacts. Once connected to the bottom piece (Fig. 4.4 left picture), holding the sample, the spring contacts make an electrical connection to the contact pads which are lithographically defined on the sample.

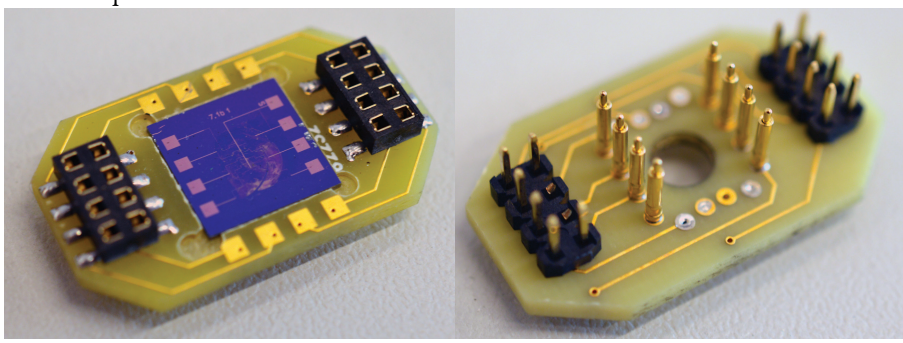

**Fig. 4.4:** Pictures of both sides of the chip carrier, left shows the bottom piece holding the sample, right shows the top piece with the spring contacts. The top is connected to the bottom part and the spring contacts facilitate the electrical connection between the sample and the carrier. The carrier is then connected to the insert.

## 4.2 Measurement electronics

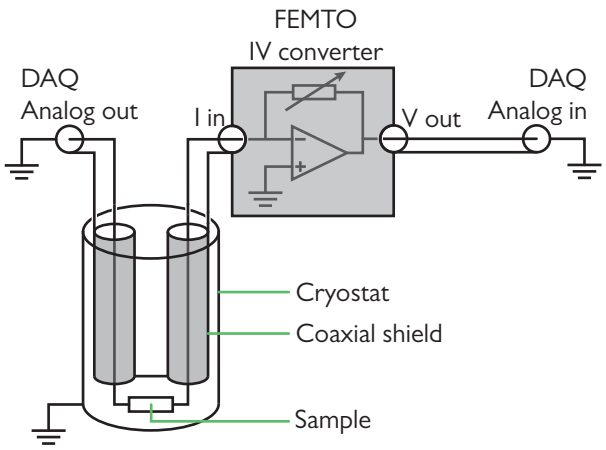


**Fig. 4.5:** Wiring schematic of a sample in the cryostat, attached to measurement electronics. A data acquisition (DAQ) card supplies a voltage to the sample, resulting in a current flowing through the sample. This current flows into the FEMTO IV converter, where it is converted to a voltage. This voltage is measured using an analog input on the same DAQ. The ground of the DAQ is connected to the shield of the coaxial voltage supply cable on the insert, which is connected to the shield of the current return line at the bottom of the insert. At the top, this shield is connected to the ground of the FEMTO, which is itself connected to the ground of the DAQ. The insert is floating inside the cryostat, and not electrically connected to it. The cryostat itself is separately grounded.

Once a sample is loaded in the cryostat, the insert is connected electrically to the measurement equipment as seen in Fig. 4.5. A NI USB 6341 DAQ (Data Acquisition card) is used to apply a bias on one end of the sample through a shielded cable. The shield of the DAQ analog out is connected to the shield of the cable. At the bottom of the insert, the shields of all cables are connected. The bias causes a current to flow, which is measured at the FEMTO DLCPA-200 IV converter. The FEMTO is connected to the insert by a doubly shielded cable, eliminating electromagnetic pick-up. In order to minimize noise introduced in the measurements, the sample is left electrically floating inside the cryostat, which means that the cryostat itself acts as a shield. The output of the FEMTO is connected to the analog input of the DAQ, which is grounded. In order to reduce high frequency noise, a 50 Hz low-pass filter can be connected between the output of the FEMTO and the input of the DAQ, but it is not depicted in the figure.

### 4.2.1 Improving noise floor

Inside the Coulomb blockade regime, the electrical current depends strongly on the applied bias. This means that in order to measure far into this regime, a very low noise floor is required. A lot of noise is suppressed by the wiring of the insert, discussed in the previous sections. However, a lower noise floor is gained by tuning the method of the current measure-

ment. The measurement is done in a two-point fashion, meaning that there is one output voltage and consequently a flowing current which is measured. In order to discern capacitive effects from resistive ones, the voltage is varied in a trace-retrace fashion. By varying the output voltage following a triangle wave (as seen in Fig. 4.6, left plot), multiple of these measurements are done in series. Typical frequencies vary between a few Hz and a few mHz. To anticipate the non-linear dependence of the current on voltage, the output voltage is evenly spaced on a log-scale, this means that the triangle wave only has a triangle shape on a logarithmic plot. After half a period, the voltage is inverted and the triangle wave is repeated, resulting in the plot shown.

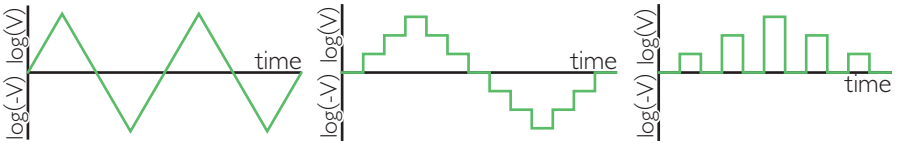


**Fig. 4.6:** DAQ output voltage versus time. The output voltages are evenly spaced logarithmically. Left: two trace-retrace voltage outputs in series The multiple trace-retrace measurements are averaged. Middle: zoom in on one trace-retrace output. From here, it can be seen that the trace-retrace measurement is actually a series of steps. Each step consists of a large number of individual measurements, depending on the duration of each step. Right: a zoom of the middle graph. A reference measurement at zero output voltage is taken after every measurement, allowing us to correct for drift or non-ideal behavior of the IV-converter.

The individual measurements however, are done in DC. To see why, consider Fig. 4.6, center plot. The output voltage is varied in steps at a fixed time interval. At each step, the DC current is measured at a rate of 500 000 samples per second[†]. The measured data is put through a digital low-pass filter with a cut-off frequency that is ten times larger than the voltage varying rate. This removes high frequency noise, while retaining a quick response necessary for the sharp voltage steps. The data is then averaged and saved. In order to correct for voltage drift (for example due to sample heater currents flowing down the insert next to the measurement wires), the voltage is set to zero after each measurement (see Fig. 4.6, right plot). The drift is subtracted from the signal, yielding the current.

[†] It is interesting to note here that since the noise floor of the system is 10 fA (as explained later), the amount of electrons flowing at these currents is around 50 000 $s^{-1}$. This means that on average, only one out of ten measurements includes the detection of an electron at these low currents. One might think that an electron multiplier instead of a commercially available DAQ would be more suitable for this research!

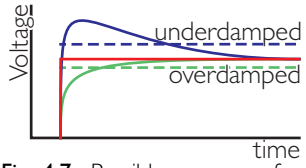


**Fig. 4.7:** Possible responses for an IV-converter (voltage versus time). Red is the ideal response. Blue is an underdamped response, resulting in a higher average measurement. Green is an overdamped response, giving a lower average measurement. The FEMTO DLCPA-200 gives an underdamped response.

Additional error is introduced by the FEMTO DLCPA-200 IV converter. It has a non-ideal response curve, which means that the output voltage of the FEMTO does not immediately settle to the correct value. This behaviour is schematically depicted in Fig. 4.7. The red line is the ideal response. Green is an overdamped case, which causes a lower average signal, seen as the dashed lines. Blue shows an underdamped case, resulting in a larger average signal. Especially at large amplification factors ($10^9$ V/A), the FEMTO shows an underdamped response, resulting in larger measured current than is actually flowing. This is corrected for in two ways. The first correction is a delay in the start of the current measurement. After setting a voltage over the sample, the FEMTO is given time to settle. The settling time is always one third of the voltage step duration. The settling of the FEMTO removes most of the overshoot, although it does not remove it completely.

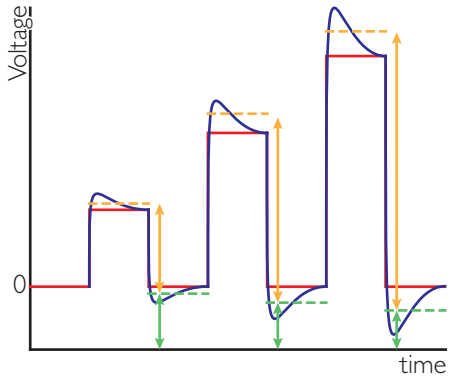


**Fig. 4.8:** Schematic voltage response of the FEMTO DLCPA-200 versus time time. Red is the ideal response. The FEMTO output has an offset due to a static input current. Blue is the measured voltage response of the FEMTO, which has an overshoot, causing a higher measured average (yellow arrows, average is yellow dashed lines). This overshoot increases with increasing input voltage, resulting from the reference measurement done after each step. However, since the same overshoot happens at the reference, the measured reference current (average in green dashed lines, arrows indicating magnitude) decreases with increasing voltage.

The second method is a correction done after the measurement. Consider the response curve shown in Fig. 4.8, which shows the response of the FEMTO as a function of time. The red curve shows the ideal response, the actual response is shown in blue. As can be seen in the curve, the reference signal is measured after each voltage step, as also seen in Fig. 4.6, right plot. The average of the reference measurement (dashed green line, green arrow) is subtracted from the signal (yellow dashed line) to obtain the recorded current, seen as the yellow arrow. However, due to the overshoot, this recorded current is larger than the true

current entering the FEMTO. More specifically, this overshoot is added twice, once due to the overshoot in the signal, and once due to the subtraction of the reference signal. This is supported by plotting the reference signal as a function of the set voltage before the reference measurement, seen in Fig. 4.9.

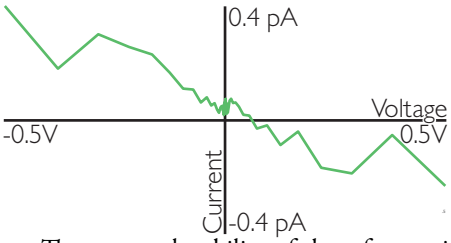


**Fig. 4.9:** Reference current (at zero volts) as a function of the voltage in the previous measurement. The line is the average taken over ten identical measurements. From the plot, it can be seen that the slope is negative, in agreement with Fig. 4.8, green arrows.

The temporal stability of the reference is important, since it allows us to extract the overshoot of the FEMTO exactly. As seen in Fig. 4.9, the reference signal is simply the sum of the overshoot and an arbitrary zero. This zero is in principle an adjustable parameter in the FEMTO IV-converter. In practice, however, it is easier to correct for this during data analysis, rather than correcting it manually before each measurement. Taking the mean of the drift current gives this zero, and subtracting it from the signal yields the overshoot. This overshoot is added twice[‡], yielding the current flowing through the device. Using these corrections in addition to large measurement times and doing repeated trace-retrace measurements, it is possible to achieve a noisefloor of under 10 fA, using 30 min averaging time per voltage step.

[‡] The overshoot extracted from the reference measurement has opposite sign, compared to the overshoot in the real signal, hence it is added and not subtracted.

## 4.3 Sample fabrication

Studying electron transport through networks of nanoparticles at low temperatures does not only require measurement apparatus, it also requires proper samples. Furthermore, these networks should somehow be connected to the equipment in order to be studied. This section first describes the fabrication of the devices used to connect the networks to the environment, and subsequently discusses the actual synthesis of the networks themselves.

### 4.3.1 Device fabrication

As was mentioned in the previous section, the current through Coulomb blockaded nanoparticle networks is very small. With this in mind, a device structure with a very large aspect ratio (length divided by width) was designed. A device like this measures many parts of the nanoparticle network in parallel, ideally increasing the total current, by four orders of magnitude in this case. A device like this would be very long, as with an aspect ratio of 10 000, a device width of 500 nm results in a length of 5 mm! These geometries are difficult to fabricate accurately using lithography (and also give problems with space on the sample), and hence the device was folded up to create the interdigitated structure shown in Fig. 4.10.

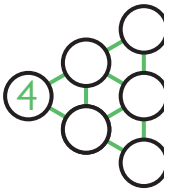


The contacts to the nanoparticle arrays were fabricated using electron beam lithography. First, a silicon wafer (P type doped with boron, 0.001 Ω m, 300 nm oxide) was diced to 1x1 cm chips. The chip is then spin coated with PMMA (polymethyl methacrylate, 950 kDa molecular weight, 4% weight in anisole) for 90 seconds at 4000 RPM to obtain a layer thickness of 250 nm. After spin coating, the chip is baked at 180 °C for 90 seconds. The baking flattens the PMMA layer and allows the anisole to evaporate.

Typically, six of these chips were simultaneously loaded in a Raith 100 EBPG electron beam lithography machine. In order to improve fabrication speed while maintaining high resolution, the patterning was done in two steps. First, small device patterns were written using a small spot size (140 nm), which functioned as the contacts to the nanoparticle networks. This was done for each loaded sample, while measuring the beam current in between samples in order to maintain the correct dose. Finally, large patterns were written using the largest available spot size (700 nm). These large patterns functioned as a connection between the measurement apparatus and the small devices on the chip. Again, the beam current was measured between each pattern, and corrections were done to the dwell time in order to maintain a constant dose. For all patterns, the acceleration voltage was kept at 30 kV. The dose was 270 $\mu C\,cm^{-2}$ for the small patterns and 300 $\mu C\,cm^{-2}$ for the large patterns[§]. Patterning was done programmatically and overnight using self-written scripts.

Development was done by submerging the chips in a 1:3 mixture of methyl isobutyl

[§]The small patterns are sensitive to the proximity effect and are given a smaller dose. This effect doesn't play an important role for the larger patterns, which hence have a larger dose. Since writing these large patterns takes much longer than writing the small patterns, this higher dose allows for fluctuations in the electron beam current.

ketone and isopropyl alcohol for 50 seconds at room temperature. The chip was then immediately transferred to pure isopropyl alcohol to stop development. The chip was removed from the solvent and blow-dried using a nitrogen gun.

After development, the chips were mounted on the sample rod of a resistance evaporator. This machine uses a high current (> 150A) to heat up chromium and gold in order to evaporate it. The chips were positioned upside down above the metals, and a 3.5 nm adhesion layer of chromium was evaporated, followed by 15 nm of gold. Deposition rate was monitored *in situ* using a quartz balance. The total thickness was chosen to be under 20 nm, to allow the network to adhere close to the contacts, as well as to the substrate itself.

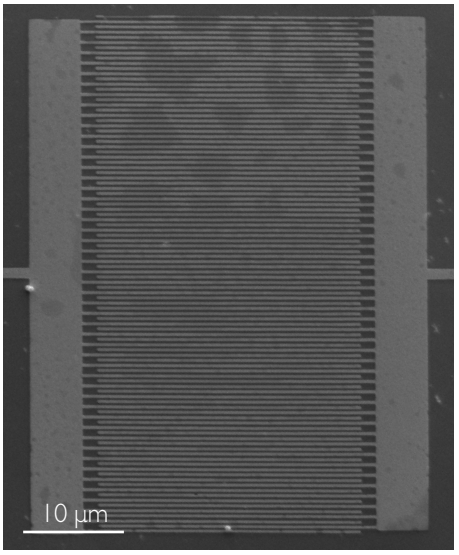


**Fig. 4.10:** Scanning electron microscopy image of a typical device structure. The device is in gold on $Si/SiO_2$ with 500 nm inter-electrode distance.

Lift-off was performed by submerging the chips in hot acetone (45 °C). After 30 minutes, the deposited metal around the edges had visibly loosened. A strong flow was created using a Pasteur pipette, which detached most of the metal from the surface. The chips were quickly transferred to a clean acetone solution and sonicated for 30 seconds to one minute. This last step removed the gold between the small gold electrodes. The chips were removed from the acetone while being sprayed with isopropyl alcohol to prevent evaporation of the acetone (evaporation of acetone leaves a visible organic layer) and subsequently blow-dried with nitrogen, yielding clean device structures as shown in Fig. 4.10.

### 4.3.2 Nanoparticle synthesis

The second step of sample fabrication is of course the synthesis of the nanoparticle networks themselves. The networks as well as the 10 nm nanoparticles (particles smaller than 10 nm were purchased at Sigma Aldrich) were synthesized in-house.

10 nm diameter gold nanoparticles were synthesized using the aqueous chemical reduction of chlorauric acid following a synthesis method pioneered by Turkevich[2] and later refined by Frens *et al.*[3] and Slot *et al.*[4]. Slot *et al.* used two competing reducing agents (trisodium citrate and tannic acid), where the growth is initially seeded by both reducing agents, but the growth itself is controlled exclusively by trisodium citrate[5]. Briefly: 10 mg of $HAuCl_4 \cdot 3H_2O$ (Aldrich) was dissolved in 100 mL demiwater (18 MΩ cm, Millipore)

and heated to 60 °C to which 40 mg of trisodium citrate (Aldrich) and 800 μg of tannic acid (Aldrich) were added under vigorous stirring as reducing agents. After two minutes, the solution had turned dark red and was heated to a boil under reflux while stirring vigorously. After ten minutes, the solution had turned ruby red and was cooled to room temperature. The nanoparticles were separated from the solvent by centrifugation (10 °C, 15000 RPM, 60 min) and the supernate was removed. The nanoparticles were redispersed in absolute ethanol (Aldrich) and 100 μL of the desired alkanethiol was added. The resulting solution was stored in the fridge to precipitate over the course of one to three days. The supernate was removed and the nanoparticles were redispersed in 0.4 ml of chloroform (Aldrich) for every ml of supernate removed. The nanoparticle size was checked under a scanning electron microscope.

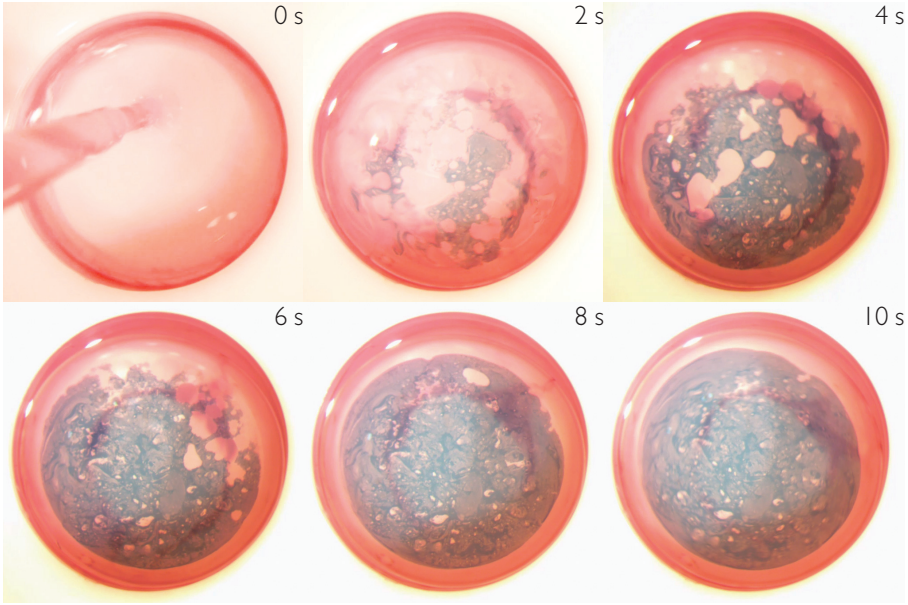


**Fig. 4.11:** Optical images of a nanoparticle array forming on a water surface in a PTFE cup. Top left is the first image and bottom right is the final image. Top left: a solution of alkanethiol capped gold nanoparticles in chloroform is pipetted onto a convex water surface. Top center: the chloroform starts to evaporate and a array quickly forms. Top right: the array grows quickly from the edges outwards. Bottom left: the array starts filling the PTFE cup, and further growth on the edges compresses the array. Bottom center: holes in the array are closed due to compression. Bottom right: the array finished growing and almost completely covers the water surface.

For nanoparticle array fabrication, a 50 μL of gold nanoparticle solution in chloroform

was added to the convex water surface in a PTFE beaker. After evaporation of the solvent, a gold nanoparticle array can be seen floating on the surface (this process is shown in Fig. 4.11). Transfer to lithographically defined devices (500 nm interelectrode spacing, 5 mm device length, Fig. 4.10, discussed in the previous section) on a diced silicon wafer (300 nm oxide) was done by a PDMS stamp. The stamp was cut to a small size, allowing full coverage of all devices, but not covering much more of the sample, allowing comparison to a bare reference device, which should not allow a current to flow. The stamp was slowly lowered to the surface of the water, allowing it to touch. After a few seconds of contact (this time did not seem to be crucial), the stamp was quickly removed from the water surface, possibly leaving water droplets on the stamp. The stamp was blow-dried with nitrogen, after which the nanoparticle array can be seen on the stamp. It was subsequently lowered onto the substrate using tweezers, and light pressure was applied by hand. The stamp was removed, leaving the array stuck to the substrate. An optical image of such a sample, including a SEM image can be seen in Fig. 4.12.

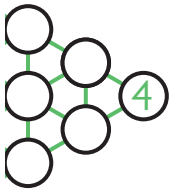


Preliminary characterization of the arrays was done by measuring the room temperature two-probe resistance of all the devices on the sample. This allowed us to eliminate devices where the lift-off was unsuccessful, resulting in a shorted device, or devices where the nanoparticle array did not attach and left an open circuit.

Other methods of nanoparticle synthesis and array fabrication were attempted, such as the method proposed by Martin *et al.* [6], as this would provide easy means to synthesize smaller nanoparticle but also improve array quality. Although the nanoparticle synthesis itself looked successful by eye, SEM inspection could not give clear insights on this, as the resolution of the SEM was not good enough. The array synthesis using these nanoparticles was unsuccessful, as deposition of the solution of nanoparticles in hexane on the toluene droplet simply caused the droplet to disperse, instead of leaving it covered with the nanoparticle solution. An alternative was tried, where instead of nanoparticles in hexane, we used nanoparticles dissolved in chloroform. This however gave the same result as the hexane solution.

An alternative to the array formation on the water surface in a teflon cup, is a droplet-drying method proposed by Lin *et al.* [7], which results in extremely long-range-ordered nanoparticle arrays, with single-crystalline domains of over a few micrometers.

This method was tried with 10 nm nanoparticles on $SiO_2$ as well as on teflon using both toluene and chloroform as a solvent. However, even tuning the volume fraction of excess thiol in the solution between $10^{-4}$ and $10^{-2}$ did not show the formation of ordered arrays, but instead showed a coffee-stain-like effect.

After the arrays have been fabricated, they can be interconnected by the molecule of interest using molecular place-exchange, creating a network. The sample is put into a solution (usually a concentration of roughly 1mM, but can vary by an order of magnitude) of the molecule overnight (the time depends on the concentration and commonly varies between one and 24 hours). During this time, the alkane thiols can de-attach from the nanoparticles,

allowing the molecule to bind to the nanoparticle by a sulfur bond. In the case of dithiols, the other end of the molecule can bind chemically to the other nanoparticle. After place exchange, the resistance of the device has usually dropped by a few orders of magnitude, depending on the alkanethiol and the exchanged molecule, as already seen in Fig. 2.9.

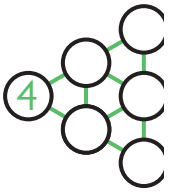

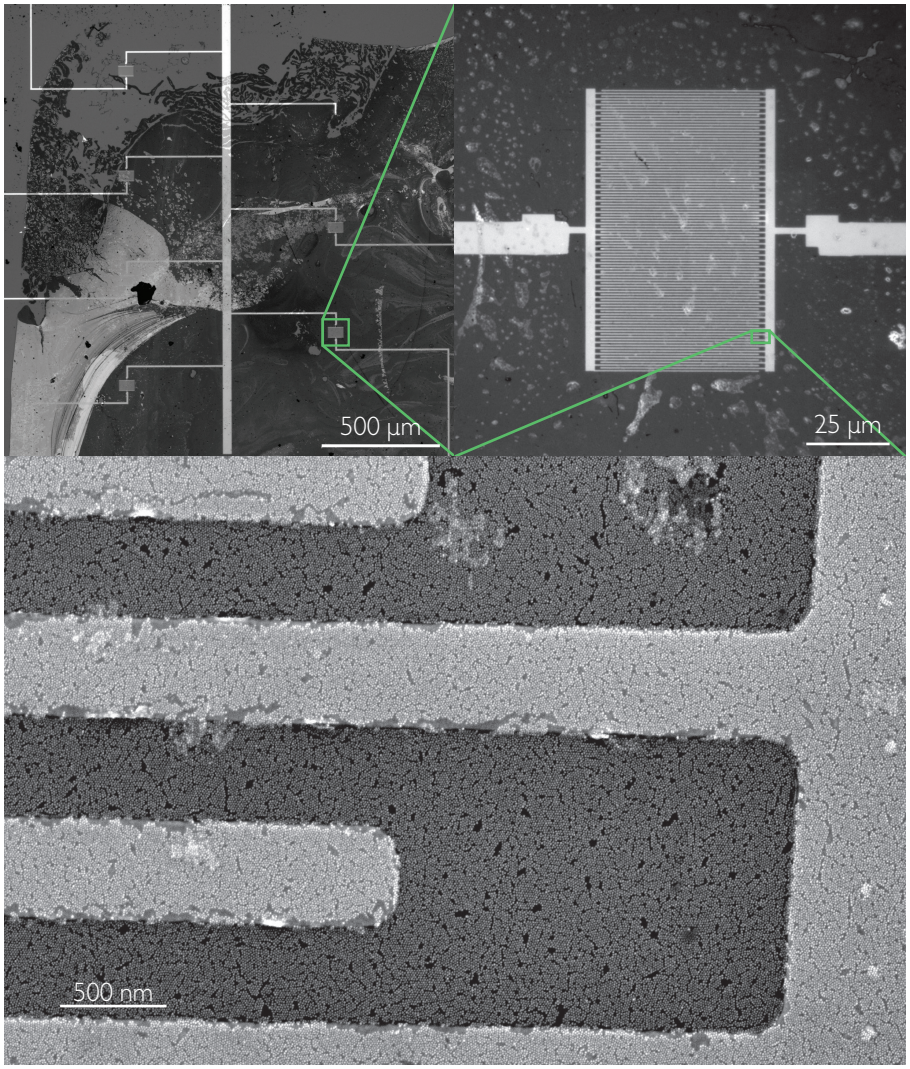


**Fig. 4.12:** Images of a sample containing devices with a gold nanoparticle array stamped on top. Top two images are obtained using an optical microscope, bottom image is a SEM picture. These images nicely illustrate the different length scales involved; from the large structures on the top left, just visible to the naked eye, to the meandering device structure, just barely resolved by visible light, to the array of tiny nanoparticles between the electrodes. The top left image shows the large device structure of the gold contact lines connecting to the devices seen on the top right. The bottom image shows that multiple crystal domains of the array are present between the gold contacts.

# References

[1] Isabelle Heukensfeldt Jansen. Analyzing multiple cotunneling distance for gold nanoparticle arrays at cryogenic temperatures. Master's thesis, Leiden University, 2016.

[2] John Turkevich, Peter Cooper Stevenson, and James Hillier. A study of the nucleation and growth processes in the synthesis of colloidal gold. *Discussions of the Faraday Society*, 11:55–75, 1951.

[3] G. Frens. Controlled nucleation for the regulation of the particle size in monodisperse gold suspensions. *Nature Physical Science*, 241:20, 1973.

[4] J. W. Slot and Hans J. Geuze. A new method of preparing gold probes for multiple-labeling cytochemistry. *European Journal for Cell Biology*, 38(1):87–93, 1985.

[5] Jordi Piella, Neus G. Bastús, and Victor Puntes. Size-Controlled Synthesis of Sub-10-nanometer Citrate-Stabilized Gold Nanoparticles and Related Optical Properties. *Chemistry of Materials*, 28(4):1066–1075, 2016.

[6] Matthew N. Martin, James I. Basham, Paul Chando, and Sang-Kee Eah. Charged Gold Nanoparticles in Non-Polar Solvents: 10-min Synthesis and 2d Self-Assembly. *Langmuir*, 26(10):7410–7417, 2010.

[7] X. M. Lin, H. M. Jaeger, C. M. Sorensen, and K. J. Klabunde. Formation of Long-Range-Ordered Nanocrystal Superlattices on Silicon Nitride Substrates. *The Journal of Physical Chemistry B*, 105(17):3353–3357, 2001.